Detecting topological superconductivity with φ_0 Josephson junctions

Constantin Schrade, Silas Hoffman, and Daniel Loss
Department of Physics, University of Basel, Klingelbergstrasse 82, CH-4056 Basel, Switzerland
(Received 23 December 2016; published 19 May 2017)

The recent experimental discovery of φ_0 Josephson junctions by Szombati *et al.* [Nat. Phys. **12**, 568 (2016)], characterized by a finite phase offset in the supercurrent, requires the same ingredients as topological superconductors, which suggests a profound connection between these two distinct phenomena. Here, we show that a quantum dot φ_0 Josephson junction can serve as a qualitative indicator for topological superconductivity: microscopically, we find that the phase shift in a junction of s-wave superconductors is due to the spin-orbit induced mixing of singly occupied states on the quantum dot, while for a topological superconductor junction it is due to singlet-triplet mixing. Because of this important difference, when the spin-orbit vector of the quantum dot and the external Zeeman field are orthogonal, the s-wave superconductors form a π Josephson junction, while the topological superconductors have a finite offset φ_0 by which topological superconductivity can be distinguished from conventional superconductivity. Our prediction can be immediately tested in nanowire systems currently used for Majorana fermion experiments and thus offers a realistic approach for detecting topological bound states.

DOI: 10.1103/PhysRevB.95.195421

I. INTRODUCTION

Non-Abelian anyons are the building blocks of topological quantum computers [1]. The simplest realization of non-Abelian anyons are Majorana bound states (MBSs) in topological superconductors (TSs) [2]. Such a TS can be induced by an s-wave superconductor (SC) in systems of nanowires with spin-orbit interaction (SOI) subject to a Zeeman field [3–6], in chains of magnetic atoms [7–10], and in topological insulators [11–16]. However, providing experimental evidence for the existence of this new phase of matter has remained a major challenge.

Here we present a qualitative indicator of MBS based on φ_0 Josephson junctions (φ_0JJs). In φ_0JJs the Josephson current is offset by a finite phase, φ_0, so that a finite supercurrent flows even when the phase difference between the superconducting leads and the magnetic flux enclosed by the Josephson junction (JJ) vanishes. Such φ_0JJs have been discussed in systems based on unconventional superconductors [17–22], ferromagnets [23–26], quantum point contacts [27], topological insulators [28], nanowires [29–31], diffusive systems [32,33], and in Josephson junctions with alternating critical current density [34]. Recently, the connection between φ_0JJs based on nanowires and TSs has been discussed and a quantitative enhancement of the anomalous current was predicted for the topological phase [35]. Most relevant for the present work, the emergence of a φ_0JJ was theoretically predicted [36–38] in a system of a quantum dot (QD) with SOI subject to a Zeeman field when coupled to s-wave superconducting leads and observed in recent experiments [39]. Interestingly, the ingredients for observing a φ_0JJ in this type of system largely overlap with those required to generate MBSs. Therefore, it is expected that φ_0JJ can provide a platform for detecting the effects of topological superconductivity.

In this work, we focus on two models for φ_0JJs based on QDs which, compared to previous studies [36–38], are in the singlet-triplet anticrossing regime. In the first model, two s-wave SCs are tunnel coupled via a two-orbital QD with SOI and subject to a Zeeman field, see Fig. 1(a), wherein we find a finite phase shift caused by the SOI-induced mixing of singly occupied states of the QD. In the second model, replacing the two s-wave SCs by two TSs, see Fig. 1(b), we again find a finite phase shift which results from the singlet-triplet mixing of the doubly occupied QD states. When the spin-orbit vector $\mathbf{\Omega}_\mathrm{D}$ and the magnetic field are orthogonal, the system is invariant under a composition of time reversal and mirroring in the plane perpendicular to $\mathbf{\Omega}_\mathrm{D}$, under which the superconducting phase goes to opposite itself; because the energy must be invariant under this symmetry, there can be no terms that are odd in the superconducting phase difference in the Hamiltonian and thus no nontrivial phase offset [24,40]. However, the MBSs in the TS leads are not time-reversal invariant and thus transform nontrivially under the above transformations. Consequently, we anticipate a nonzero phase shift for this case. Indeed, we show that the phase shift φ_0 is equal to π for the s-wave superconducting leads [41], while $\varphi_0 \neq 0,\pi$ for the TSs leads (unlike [42,43]), which can, consequently, be used as a qualitative indicator of MBSs.

II. JOSEPHSON JUNCTION MODELS

Our starting point for both of the JJ models outlined above is the Hamiltonian

$$H_\nu = H_\mathrm{D} + H_{\nu,\mathrm{L}} + H_{\nu,\mathrm{t}}, \tag{1}$$

where $\nu = \mathrm{S,TS}$ corresponds to the model with s-wave SC leads and TS leads, respectively. The first term in this expression $H_\mathrm{D} = H_0 + H_\mathrm{Z} + H_\mathrm{SOI}$ is the Hamiltonian of an isolated QD. Here, $H_0 = (V_g + \delta/2)n_a + (V_g - \delta/2)n_b + U/2\sum_\tau n_\tau(n_\tau - 1) + U_{ab}n_a n_b$ describes a QD with two orbitals $\tau = a,b$ at energy difference $\delta > 0$ with respect to a gate voltage V_g. The particle number operator of orbital τ is $n_\tau = \sum_s d^\dagger_{\tau s} d_{\tau s}$ with $d_{\tau s}$ the electron annihilation operator with spin $s = \uparrow,\downarrow$ quantized along the z axis in orbital τ. The intraorbital (interorbital) Coulomb interaction strength is U (U_{ab}). Furthermore, $H_\mathrm{Z} = -g\mu_B B\sum_\tau(d^\dagger_{\tau\uparrow}d_{\tau\uparrow} - d^\dagger_{\tau\downarrow}d_{\tau\downarrow})/2$ describes a Zeeman field $\boldsymbol{B}$ along the z axis of magnitude

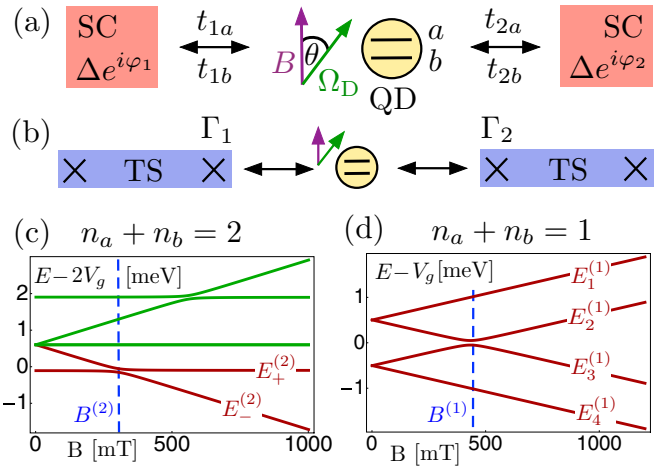

FIG. 1. Setups for φ_0JJs. (a) Two s-wave SCs (red) are tunnel coupled via a QD (yellow) with two orbitals a and b. The QD is subject to an external magnetic field $\boldsymbol{B}$ at some relative angle θ to its SOI $\boldsymbol{\Omega}_D$. (b) Same visual encodings. The SCs are replaced by two TSs (blue). The QD now couples to the two inner MBS (crosses) $\Gamma_{1,2}$ of the TSs. (c) Spectrum of the bare QD as a function of B for the double occupancy sector. Red bands contribute to our effective description; green bands do not. We have chosen $\delta = 1$ meV, $g = 40$, $U = 0.9$ meV, and $U_{ab} = 0.6$ meV, $\Omega_D = 0.1$ meV, so that $B^{(2)} = 302$ mT. (d) Same as (c) but for the single occupancy sector with $B^{(1)} = 432$ mT.

$B = |\boldsymbol{B}|$ with g the electron g factor and μ_B the Bohr magneton. Lastly, $H_{\rm SOI} = i\boldsymbol{\Omega}_D/2 \cdot \sum_{s,s'}(d_{bs}^\dagger \boldsymbol{\sigma}_{ss'} d_{as'} - \text{H.c.})$ describes the SOI on the QD, where $\boldsymbol{\Omega}_D = \Omega_D(\sin\theta, 0, \cos\theta)$, in which $\Omega_D \neq 0$, $\theta \in [0,\pi]$ is the angle of the SOI vector with respect to the Zeeman field and $\boldsymbol{\sigma}$ is the vector of Pauli matrices.

The second term in Eq. (1) describes the isolated superconducting leads. For the first model, $H_{\rm S,L} = \sum_{\eta,\mathbf{k}\sigma} E_{\mathbf{k}} \gamma_{\eta,\mathbf{k}\sigma}^\dagger \gamma_{\eta,\mathbf{k}\sigma}$, where $\gamma_{\eta,\mathbf{k}\sigma}$ is the quasiparticle annihilation operator in SC $\eta = 1,2$ with momentum $\mathbf{k}$, pseudospin $\sigma = \Uparrow, \Downarrow$, and energy $E_{\mathbf{k}} = \sqrt{\xi_{\mathbf{k}}^2 + \Delta^2}$ with Δ the superconducting gap and $\xi_{\mathbf{k}}$ the single-electron dispersion relation in the normal metal state. The nondegenerate ground state of the s-wave superconductors, $|0_\eta\rangle$, is defined so that $\gamma_{\eta,\mathbf{k}\sigma}|0_\eta\rangle = 0$. For the second model, we assume that the localization length of the MBS wave functions is much smaller than the length of TSs. We also neglect contributions of bulk quasiparticles which are valid for energies much smaller than the energy gap. Consequently the MBSs are at zero energy and $H_{\rm TS,L} = 0$. Hence the ground state of the TS leads is fourfold degenerate which, upon choosing a fixed parity subspace, becomes twofold degenerate. In the following, we consider the odd parity subspace; however, the results for the even parity ground state subspace are identical. Finally, if the localization length of the MBS wave function is comparable to the length of the TSs, a finite energy splitting between the MBS in the same TS is induced, $H_{\rm TS,L} \neq 0$. However, within the perturbation theory approach carried out in the next section, this energy splitting only modifies the energy denominators in the effective Hamiltonian and can be neglected when it is small on the energy scale of the separation between the TS chemical potentials and the QD energy levels [44].

The last term in Eq. (1) describes the tunnel coupling between the superconducting leads and the QD. For the first model, it is given by

$$H_{\rm S,t} = \sum_{\eta\tau}\sum_{\mathbf{k}s} t_{\eta\tau} e^{i\varphi_\eta/2}\, c_{\eta,\mathbf{k}s}^\dagger d_{\tau s} + \text{H.c.}, \tag{2}$$

with $c_{\eta,\mathbf{k}s}$ being the annihilation operator of an electron with momentum $\mathbf{k}$ and spin s in SC η [45]. It is related to the quasiparticle operators by $c_{\eta,\mathbf{k}\uparrow} = u_{\mathbf{k}}\gamma_{\eta,\mathbf{k}\Uparrow} + v_{\mathbf{k}}\gamma_{\eta,-\mathbf{k}\Downarrow}^\dagger$ and $c_{\eta,-\mathbf{k}\downarrow} = u_{\mathbf{k}}\gamma_{\eta,-\mathbf{k}\Downarrow} - v_{\mathbf{k}}\gamma_{\eta,\mathbf{k}\Uparrow}^\dagger$ with coherence factors $u_{\mathbf{k}} = (1/\sqrt{2})\sqrt{1 + \xi_{\mathbf{k}}/E_{\mathbf{k}}}$ and $v_{\mathbf{k}} = (1/\sqrt{2})\sqrt{1 - \xi_{\mathbf{k}}/E_{\mathbf{k}}}$. The tunneling Hamiltonian also contains the superconducting phase φ_η of SC η and real, spin, and momentum-independent tunneling amplitudes $t_{\eta\tau}$. The more general case of spin-dependent tunneling amplitudes does not alter our results (see also Appendixes B and C). For the second model, the coupling of the TSs and the QD is given by

$$H_{\rm TS,t} = \sum_{\eta\tau}\sum_{s} t_{\eta\tau} e^{i\varphi_\eta/2}\, \Gamma_\eta d_{\tau s} + \text{H.c.}, \tag{3}$$

with Γ_η being the MBS in TS η which is spatially closest to the QD [46–48]. We assume that its partner Γ_η' at the opposite end of the TS does not couple to the QD. However, they form nonlocal fermionic operators $C_1 = (\Gamma_1' + i\Gamma_1)/2$ and $C_2 = (\Gamma_2 + i\Gamma_2')/2$. Additionally, we assume temperatures that are smaller than the superconducting gap Δ and the separation between the MBS and the next finite-energy Andreev bound state Δ', $k_BT \ll \Delta, \Delta'$.

We now proceed with a discussion of $H_{\rm D}$ in the regime of $\delta > U > U_{AB} \gg |\Omega_D|$ common to typical experiments [39]. First, we address the case of a doubly occupied dot, $n_a + n_b = 2$. For $\Omega_D = 0$, the spectrum consists of three singlet (triplet) bands which are constant (split) as a function of the Zeeman field. As experimentally observed in [49], for finite Ω_D and θ, the singlet and triplet bands anticross; see Fig. 1(c). In all following discussions, we operate the QD in the regime close to the anticrossing of the singlet $|S\rangle = d_{b\uparrow}^\dagger d_{b\downarrow}^\dagger |0_D\rangle$ and the triplet $|T\rangle = d_{a\uparrow}^\dagger d_{b\uparrow}^\dagger |0_D\rangle$, which occurs at the Zeeman field $B^{(2)} = (\delta - U + U_{ab})/g\mu_B$. Here, $|0_D\rangle$ is the vacuum state on the dot. The effective Hamiltonian, valid to lowest order in Ω_D, which acts in the two-level subspace spanned by $|S\rangle$ and $|T\rangle$ is $H_{\rm ST}^{(2)} = (2V_g - \delta + U)|S\rangle\langle S| + (2V_g + U_{ab} - g\mu_B B)|T\rangle\langle T| + [i\Omega_D \sin(\theta)/2|T\rangle\langle S| + \text{H.c.}]$. The spectrum of $H_{\rm ST}^{(2)}$ is given by $E_\pm^{(2)}$ with corresponding orthonormal eigenstates

$$|E_\pm^{(2)}\rangle = iS_\pm|S\rangle + T_\pm|T\rangle. \tag{4}$$

Here, $S_\pm, T_\pm$ are real functions of the system parameters; see also Appendix A.

Second, we discuss the case of a singly occupied dot, $n_a + n_b = 1$. For $\Omega_D = 0$, the energy levels for opposite spins split as a function of the Zeeman field. For finite Ω_D and θ, an energy gap opens up at the crossing point $B^{(1)} = \delta/g\mu_B$ of the spin-up band in orbital a and the spin-down band in orbital b; see Fig. 1(d). We will denote the four eigenvalues of the singly occupied sector by $E_\lambda^{(1)}$ for $\lambda = 1, \ldots, 4$. The corresponding

orthonormal eigenstates are given by

$$|E_\lambda^{(1)}\rangle = \sum_s (i A_{\lambda s} d_{as}^\dagger + B_{\lambda s} d_{bs}^\dagger)|0_D\rangle. \quad (5)$$

Here, $A_{\lambda s}$, $B_{\lambda s}$ are real functions of the system parameters; see Appendix A. The relative imaginary unit in both Eq. (4) and Eq. (5) is due to the SOI. We adjust the filling and the gate voltage of the QD, so that its ground state is given by $E_-^{(2)}$ while its first excited states are given by $E_+^{(2)}$ and $E_\lambda^{(1)}$ for some fixed λ. The separation between $E_-^{(2)}$ to the states $E_{\lambda'}^{(1)}$ with $\lambda' \neq \lambda$ is assumed to be large, $|E_{\lambda'}^{(1)} - E_-^{(2)}| \gg E_\lambda^{(1)} - E_-^{(2)}$. Finally, the remaining occupancy sectors of the QD, whose energies are much larger than the QD-lead coupling, are not relevant for our results and are hence omitted.

III. DETECTING TOPOLOGICAL SUPERCONDUCTIVITY

In order to calculate the superconducting current, we tune the chemical potential of the superconductors close to the $E_-^{(2)}$ level. We require for the SC JJ that $\pi \nu_F t_{\eta\tau} t_{\eta'\tau'} \ll E_\lambda^{(1)} - E_-^{(2)}, |\Omega_D| \sin(\theta), \Delta$ with ν_F the normal-state density of states of the leads at the Fermi energy and for the TS JJ that $t_{\eta\tau} \ll E_\lambda^{(1)} - E_-^{(2)}, |\Omega_D| \sin(\theta)$, so that in both cases the states $E_+^{(2)}$ and $E_\lambda^{(1)}$ on the QD serve as virtual tunneling states. Our approach is valid for angles $\theta \in [\theta_c, \pi - \theta_c]$, where θ_c is a critical angle determined by the conditions above; see also Appendix D. Furthermore, we work in a temperature regime of $k_B T \ll E_\lambda^{(1)} - E_-^{(2)}, |\Omega_D| \sin(\theta)$. The effective tunneling Hamiltonian $H_{S,t}$ ($H_{TS,t}$) valid up to fourth (second) order in the tunneling amplitudes acting on the ground state of the isolated dot and s-wave (odd parity) ground state of the uncoupled leads is

$$H_{\nu,t}^{\text{eff}} = \left(E_\nu^0 \cos\varphi_\nu + E_\nu^a \sin\varphi_\nu\right) T_\nu + \widetilde{E}_\nu, \quad (6)$$

with $\varphi_S = 2\varphi_{TS} = \varphi_1 - \varphi_2$ and $T_S = 1$, $T_{TS} = C_1^\dagger C_2 + \text{H.c.} = i\Gamma_2\Gamma_1$ [44]. The first term in Eq. (6) arises due to Cooper pair (nonlocal fermion) tunneling across the (TS) SC JJ. The second term is an energy offset, due to processes for which there is no such transport. At zero temperature, the Josephson current, defined by $I_\nu = 2e\partial_\varphi E_{\nu,GS}/\hbar$ with $E_{\nu,GS}$ the ground state energy of the coupled system, is given by

$$I_\nu = -I_\nu^c \sin\left(\varphi_\nu - \varphi_\nu^0\right), \quad \varphi_\nu^0 = \arctan\left(E_\nu^a / E_\nu^0\right), \quad (7)$$

where the critical current is $I_\nu^c = 2\kappa_\nu e\sqrt{(E_\nu^0)^2 + (E_\nu^a)^2}\,\text{sgn}(E_\nu^0)/\hbar$. Because in the TS case the ground state is a function of φ, the sign of the Josephson energy also depends on the phase difference: $\kappa_{TS} = -1/2$ when $-E_{TS}^0 \cos\varphi_{TS} - E_{TS}^a \sin\varphi_\nu + \widetilde{E}_{TS}$ is the ground state energy and $\kappa_{TS} = 1/2$ otherwise. In the SC case the ground state is independent of φ and therefore $\kappa_S = 1$. Notice that there is a finite phase shift only when $E_\nu^a \neq 0$. For the BCS JJ the coefficients in Eq. (6) are given by

$$\begin{aligned} E_S^0 &= g_S t_{1b} t_{2b} B_{\lambda\uparrow}^2 \left(A_{\lambda\uparrow}^2 t_{1b} t_{2b} + B_{\lambda\uparrow}^2 t_{1a} t_{2a}\right), \\ E_S^a &= g_S t_{1b} t_{2b} A_{\lambda\uparrow} B_{\lambda\uparrow}^3 (t_{1a} t_{2b} - t_{1b} t_{2a}). \end{aligned} \quad (8)$$

The prefactor $g_S > 0$, which is not relevant for the phase shift φ_S^0, includes the coherence factors and energy denominators picked up in the perturbation theory; see also Appendix B.

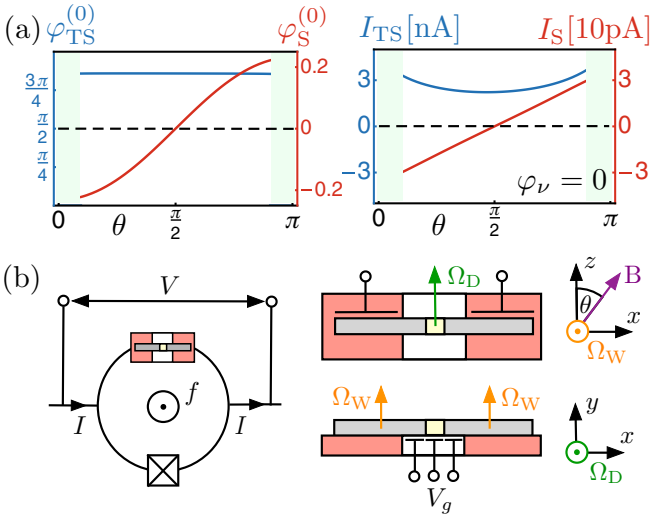

FIG. 2. (a) Phase shift $\varphi_\nu^0(\theta)$ (left panel) and Josephson current $I_\nu(\theta)$ at $\varphi_\nu = 0$ (right panel) for $\lambda = 4$ and $\theta \in [\theta_c, \pi - \theta_c]$ with $\theta_c = 0.3$. System parameters are chosen as in Fig. 1 with $B = B^{(2)}$, $V_g = -0.80$ meV, $t_{1a} = t_{2b} = 0.01$ meV, $t_{1b} = 0.05$ meV, and $t_{2a} = 0.04$ meV. Compared to the SC JJ the phase shift (Josephson current at $\varphi_S = 0$) is nonzero for the TS JJ. (b) Experimental proposal. Left panel: SQUID geometry of a nanowire QD JJ and a reference junction without a QD connected in parallel. The current-phase relation of the Josephson current through the QD JJ is measured with respect to the reference junction by tuning the flux f through the SQUID. Right panel: top view (upper panel) and side view (lower panel) of the QD JJ. Local gates are applied to define the tunnel coupled QD (yellow) as a short segment in a nanowire (gray) which is proximity-coupled to an s-wave SC (red). Local gates are also used to orient the dot SOI $\mathbf{\Omega}_D$ (green) and wire SOI $\mathbf{\Omega}_W$ (orange), respectively. To measure $\varphi_\nu^0(\theta)$ and $I_\nu(\theta)$, a magnetic field $\mathbf{B}$ is rotated in the plane parallel to the SC film.

The SC JJ exhibits in general a finite phase shift, when $t_{1a}t_{2b} - t_{1b}t_{2a} \neq 0$. For $\varphi_S = 0$, the sign of the supercurrent is determined by $\text{sgn}(t_{1a}t_{2b} - t_{1b}t_{2a})$ and $\text{sgn}(A_{\lambda\uparrow}B_{\lambda\uparrow}) \propto \text{sgn}(\Omega_D)$. The origin of the phase shift in the SC JJ is the superposition of singly occupied QD orbitals. Depending on the virtual state, an electron tunnels with amplitude $\propto i A_{\lambda\uparrow} B_{\lambda\uparrow}$ when switching orbitals on the dot or $\propto (B_{\lambda\uparrow})^2$ or $\propto (A_{\lambda\uparrow})^2$ if the orbital is constant. Thus Cooper pairs tunneling with amplitude E_S^a when the former process occurs once and amplitude E_S^0 when the process occurs an even number of times Appendix B.

Notably, when the relative angle between Zeeman field and SOI is $\theta = \pi/2$ the SOI only mixes opposite spins in different orbitals so that $A_{\lambda\uparrow} = B_{\lambda\downarrow} = 0$ for $\lambda = 1,4$ and $A_{\lambda\downarrow} = B_{\lambda\uparrow} = 0$ for $\lambda = 2,3$. Thus $E_s^a = 0$ and the phase shift φ_S^0 vanishes; see Fig. 2(a).

Unlike the SC JJ, the TS JJ allows for nonzero phase shift, see Fig. 2(a), at $\theta = \pi/2$. The coefficients in Eq. (6) for the TS JJ when $\lambda = 1,4$ are given by

$$\begin{aligned} E_{TS}^0(\pi/2) &= g_{TS} B_{\lambda\uparrow}^2 S_- T_- (t_{1b}t_{2a} - t_{1a}t_{2b}), \\ E_{TS}^a(\pi/2) &= -g_{TS} B_{\lambda\uparrow}^2 (S_-^2 t_{1b}t_{2b} + T_-^2 t_{1a}t_{2a}), \end{aligned} \quad (9)$$

where the prefactor $g_{TS} > 0$ includes the energy denominators of the perturbation theory; see also Appendix C. In comparison

to the SC JJ, the sign of the supercurrent at $\varphi_{\rm TS}=0$ in the TS JJ is determined by parity $i\Gamma_2\Gamma_1$. If the parity fluctuates, the supercurrent exhibits fluctuations as well. So the observation of a phase shift requires sufficiently long parity lifetimes which can be up to minutes [50]. Focusing on the case when $\lambda=1,4$, the processes that contribute to $E^0_{\rm TS}(\pi/2)$ in Eq. (9) come from virtual tunneling sequences taking a singlet to a triplet state, with amplitude $\propto iS_-T_-$, and the corresponding sequences taking a triplet to the singlet state, with an amplitude $\propto -iS_-T_-$. We emphasize that these processes are only possible due to the singlet-triplet mixing described in the previous section. When the order in which the nonlocal fermion is created or destroyed is opposite between these processes, the tunneling sequences differ in phase by $\varphi_{\rm TS}+\pi$ and acquire the same tunneling coefficients so that their sum is proportional to $\cos(\varphi_{\rm TS})$. Distinctly, $E^a_{\rm TS}(\pi/2)$ originates from sequences that take the singlet ($\propto S^2_-$) or triplet ($\propto T^2_-$) to itself. In both cases there exist two sequences that, again, differ in phase by $\varphi_{\rm TS}+\pi$ but have the same tunneling coefficients, so that their sums are $\propto\sin(\varphi_{\rm TS})$. When $B\gg B^{(2)}$ or $\lambda=2,3$, $E^0_{\rm TS}=0$ and we obtain a $\varphi^0_{\rm TS}=\pi/2$ JJ for TS.

IV. EXPERIMENTAL PROPOSAL

In this section, we propose an experiment similar to [39] for detecting topological superconductivity using a QD φ_0JJ. We consider a nanowire (NW) which is aligned along the x direction and proximity-coupled to an s-wave SC; see Fig. 2(b). By using local bottom gates, we form a tunnel coupled QD as a short slice in the wire. The electric field produced by the gates points along the y direction, so that the dot SOI $\mathbf{\Omega}_{\rm D}$ points along the z direction. Furthermore, we contact the wire segments with back gates that generate electric fields along the z direction and consequently induce a wire SOI $\mathbf{\Omega}_{\rm W}$ that points along the y direction. We also apply an external magnetic field $\mathbf{B}$ that can be rotated in the xz plane. Alternatively, the external magnetic field $\mathbf{B}$ is kept fixed and the sample is rotated. Finally, we connect the resulting QD JJ to a reference junction without a QD forming a SQUID geometry. By tuning the flux f through the SQUID, the current-phase relation of the QD JJ and consequently the anomalous phase shift can be measured with respect to the reference junction.

Our proposed experiment proceeds in three steps.

(1) Initialization. We adjust the size of the QD so that the singlet-triplet anticrossing occurs for a field close to the topological phase transition, $g\mu_B B^*=\sqrt{\Delta^2+\mu^2}$ with the chemical potential of the NW leads, μ, tuned to $E^{(2)}_-$. Moreover, we adjust the gate voltage V_g and filling of the QD so that its ground state is given by $E^{(2)}_-$, while its first excited states are $E^{(2)}_+$ and $E^{(1)}_4$.

(2) Trivial phase. We consider the regime of a weak Zeeman field, $B<B^*$. The NW chemical potential is placed well above the magnetic field gap. In this limit, the SOI correction to the NW dispersion is irrelevant. Also, the effect of the Zeeman field on the NW leads is negligible, as it is well below the field B^* [51]. Hence the QD JJ is described by the effective tunneling Hamiltonian $H^{\rm eff}_{S,t}$. We expect not to observe an anomalous phase shift when the magnetic field $\mathbf{B}$ and the dot SOI $\mathbf{\Omega}_{\rm D}$ are orthogonal, $\varphi^0_S(\theta=\pi/2)=0$.

(3) Topological phase. The setup is tuned to the topological phase by increasing the magnitude of the Zeeman field so that $B>B^*$. The NW chemical potential is tuned inside the magnetic field gap. A MBS emerges at the NW boundaries and the QD JJ is described by the effective tunneling Hamiltonian $H^{\rm eff}_{{\rm TS},t}$. We expect to observe a change in the phase shift of the Josephson current from $\varphi^0_S(\pi/2)=0$ to some $\varphi^0_{TS}(\pi/2)\neq 0$. The proposed setup also allows us to measure the phase shift dependence on the relative angle θ between $\mathbf{B}$ and $\mathbf{\Omega}_{\rm D}$ by rotating $\boldsymbol{B}$ in the xz plane. We note that the MBS are unaffected by this rotation because dot SOI $\mathbf{\Omega}_{\rm D}$ and the wire SOI $\mathbf{\Omega}_{\rm W}$ are always orthogonal [6]. Notably, for typical system parameters of nanowire QD JJs, we find that, at zero phase difference between the leads, $|I_S|\approx 10$ pA, while $|I_{\rm TS}|\approx 1$ nA, which corresponds to an increase by two orders of magnitude.

Finally, we remark that for a well-defined Josephson current, we consider only regions with sizable energy gap, i.e., deep inside the trivial or topological phase. In particular, at the phase boundary, the MBS delocalize and our effective theory breaks down. In general, we expect the behavior of the phase shift to be nonuniversal across the topological phase transition.

V. CONCLUSIONS

We have introduced a qualitative indicator for the detection of topological superconductivity based on a QD φ_0JJ. We found that for this setup the trivial SCs always form a πJJ, while the TSs can form a φ_0JJ with $\varphi_0\neq 0,\pi$. This change in phase shift is accompanied by a significant increase in the magnitude of the critical current. These observations can be probed by simple modifications of recent experimental setups in nanowire QD JJs [39].

ACKNOWLEDGMENTS

We acknowledge support from the Swiss NSF and NCCR QSIT. We are grateful to J. Klinovaja for useful comments.

APPENDIX A: QUANTUM DOT WITH SPIN ORBIT INTERACTION IN A ZEEMAN FIELD

This first section of the appendix provides a more detailed discussion of the model for an isolated QD with SOI subject to an external Zeeman field as given by $H_{\rm D}$ in the main text. The Hilbert space of the system is spanned by the occupation number states

$$|n_{a\uparrow},n_{a\downarrow},n_{b\uparrow},n_{b\downarrow}\rangle=(d^\dagger_{a\uparrow})^{n_{a\uparrow}}(d^\dagger_{a\downarrow})^{n_{a\downarrow}}(d^\dagger_{b\uparrow})^{n_{b\uparrow}}(d^\dagger_{b\downarrow})^{n_{b\downarrow}}|0_{\rm D}\rangle, \tag{A1}$$

where $n_{\tau s}\in\{0,1\}$ is the occupation number of an electron with spin s in orbital τ. Since the total number of electrons on the QD is conserved, we can address each sector with fixed total occupation number separately.

1. Double occupancy sector

We start with an analysis of the double occupancy sector. A basis is given by the singlet states

$$|1,1,0,0\rangle,\quad |S\rangle=|0,0,1,1\rangle,\quad (|1,0,0,1\rangle-|0,1,1,0\rangle)/\sqrt{2}, \tag{A2}$$

and the triplet states

$$|T\rangle = |1,0,1,0\rangle, \quad (|1,0,0,1\rangle + |0,1,1,0\rangle)/\sqrt{2}, \quad |0,1,0,1\rangle. \tag{A3}$$

Representing $H_{\rm D}$ in terms of these basis states we find that

$$H_{\rm D}^{(2)} = \begin{pmatrix} 2V_g+\delta+U & 0 & 0 & -i\Omega\sin(\theta)/2 & i\Omega\cos(\theta)/\sqrt{2} & i\Omega\sin(\theta)/2 \\ 0 & 2V_g-\delta+U & 0 & -i\Omega\sin(\theta)/2 & i\Omega\cos(\theta)/\sqrt{2} & i\Omega\sin(\theta)/2 \\ 0 & 0 & 2V_g+U_{ab} & 0 & 0 & 0 \\ i\Omega\sin(\theta)/2 & i\Omega\sin(\theta)/2 & 0 & 2V_g+U_{ab}-g\mu_B B & 0 & 0 \\ -i\Omega\cos(\theta)/\sqrt{2} & -i\Omega\cos(\theta)/\sqrt{2} & 0 & 0 & 2V_g+U_{ab} & 0 \\ -i\Omega\sin(\theta)/2 & -i\Omega\sin(\theta)/2 & 0 & 0 & 0 & 2V_g+U_{ab}+g\mu_B B \end{pmatrix}. \tag{A4}$$

Here, the top left 3×3 block acts on the singlet subspace, while the bottom right 3×3 block acts on the triplet subspace and the off-diagonal blocks contain the SOI which couples the singlet to the triplet subspace. The spectrum of $H_{\rm D}^{(2)}$ is depicted in Fig. 1(c) of the main text. The effective Hamiltonian, valid to lowest order in Ω, which acts in the two-level subspace spanned by $|S\rangle$ and $|T\rangle$ is

$$H_{\rm ST}^{(2)} = \begin{pmatrix} 2V_g-\delta+U & -i\Omega\sin(\theta)/2 \\ i\Omega\sin(\theta)/2 & 2V_g+U_{ab}-g\mu_B B \end{pmatrix}. \tag{A5}$$

It contains the bare energies of the singlet $|S\rangle$ and the triplet $|T\rangle$ on its diagonal. The SOI interaction then couples these levels via the off-diagonal terms. The spectrum of $H_{\rm ST}^{(2)}$ is given by

$$E_{\pm}^{(2)} = 2V_g + [(U+U_{ab}-g\mu_B B-\delta)/2] \pm \sqrt{[(U-U_{ab}+g\mu_B B-\delta)/2]^2 + (\Omega\sin(\theta)/2)^2}. \tag{A6}$$

We see that the effect of the SOI is the opening of an energy gap at the crossing point of the bare singlet and triplet energy levels. In terms of the angle between the Zeeman field and the SOI axis, the gap is maximal when $\theta=\pi/2$ and vanishes when $\theta=0$. The eigenstates of $H_{\rm ST}^{(2)}$ are

$$|E_{\pm}^{(2)}\rangle = \begin{pmatrix} iS_{\pm} \\ T_{\pm} \end{pmatrix} \Leftrightarrow |E_{\pm}^{(2)}\rangle = iS_{\pm}|S\rangle + T_{\pm}|T\rangle, \tag{A7}$$

where the coefficients are given by

$$T_{\pm} = \pm\frac{1}{\sqrt{2}}\sqrt{1 \mp \frac{U-U_{ab}+g\mu_B B-\delta}{\sqrt{(U-U_{ab}+g\mu_B B-\delta)^2+(\Omega\sin\theta)^2}}}, \quad S_- = -\mathrm{sgn}(\Omega)T_+, \quad S_+ = \mathrm{sgn}(\Omega)T_-. \tag{A8}$$

The mixing of the singlet and the triplet is minimal when $\Omega=0$ or $\theta=0$ and it is maximal when $\theta=\pi/2$.

2. Single occupancy sector

We next discuss the single occupancy sector of the QD which is spanned by the basis states

$$|1,0,0,0\rangle, \quad |0,1,0,0\rangle, \quad |0,0,1,0\rangle, \quad |0,0,0,1\rangle. \tag{A9}$$

The matrix representation of $H_{\rm D}$ in terms of these basis states is given by

$$H_{\rm D}^{(1)} = \frac{1}{2}\begin{pmatrix} 2V_g-\delta-g\mu_B B & 0 & i\Omega\cos\theta & i\Omega\sin\theta \\ 0 & 2V_g-\delta+g\mu_B B & i\Omega\sin\theta & -i\Omega\cos\theta \\ -i\Omega\cos\theta & -i\Omega\sin\theta & 2V_g+\delta-g\mu_B B & 0 \\ -i\Omega\sin\theta & i\Omega\cos\theta & 0 & 2V_g+\delta+g\mu_B B \end{pmatrix}. \tag{A10}$$

Here, the top left 2×2 block acts on the subspace of orbital b, while the bottom right 2×2 block acts on the subspace of orbital a. The off-diagonal blocks contain the SOI which couples the a orbital to the b orbital. The spectrum of $H_{\rm D}^{(1)}$ is depicted in Fig. 1(d) of the main text and is given by

$$E_{\lambda}^{(1)} = V_g + \tfrac{1}{2}(\delta_{\lambda 1}+\delta_{\lambda 2}-\delta_{\lambda 3}-\delta_{\lambda 4})\sqrt{(\Omega\sin\theta)^2 + (g\mu_B B + (\delta_{\lambda 1}-\delta_{\lambda 2}-\delta_{\lambda 3}+\delta_{\lambda 4})\sqrt{\delta^2+(\Omega\cos\theta)^2})^2}. \tag{A11}$$

Here, $\delta_{\lambda\lambda'}$ for $\lambda,\lambda'=1,\ldots,4$, is the Kronecker δ. The eigenstates of $H_{\rm D}^{(1)}$ are of the form

$$\left|E_{\lambda}^{(1)}\right\rangle = \begin{pmatrix} B_{\lambda\uparrow} \\ B_{\lambda\downarrow} \\ iA_{\lambda\uparrow} \\ iA_{\lambda\downarrow} \end{pmatrix} \Leftrightarrow \left|E_{\lambda}^{(1)}\right\rangle = \sum_s (iA_{\lambda s}d_{as}^{\dagger} + B_{\lambda s}d_{bs}^{\dagger})|0_{\rm D}\rangle. \tag{A12}$$

We now determine the coefficients $A_{\lambda s}$ and $B_{\lambda s}$ for the different relative angles θ between Zeeman field and SOI axis.

a. Zeeman field and SOI axis are orthogonal ($\theta = \pi/2$)

For $\theta = \pi/2$, the SOI is proportional to σ^x so that we expect the eigenstates of $H_{\mathrm{D}}^{(1)}$ to be linear combinations of opposite spins in different orbitals. Indeed, we find that the only coefficients which are nonzero are given by

$$\begin{aligned} B_{1\uparrow} = A_{4\downarrow} &= \frac{1}{\sqrt{2}}\sqrt{1 - \frac{g\mu_B B + \delta}{\sqrt{(g\mu_B B + \delta)^2 + \Omega^2}}}, \quad B_{4\uparrow} = -A_{1\downarrow} = \frac{\mathrm{sgn}(\Omega)}{\sqrt{2}}\sqrt{1 + \frac{g\mu_B B + \delta}{\sqrt{(g\mu_B B + \delta)^2 + \Omega^2}}}, \\ A_{3\uparrow} = -B_{2\downarrow} &= \frac{1}{\sqrt{2}}\sqrt{1 + \frac{g\mu_B B - \delta}{\sqrt{(g\mu_B B - \delta)^2 + \Omega^2}}}, \quad A_{2\uparrow} = B_{3\downarrow} = \frac{\mathrm{sgn}(\Omega)}{\sqrt{2}}\sqrt{1 - \frac{g\mu_B B - \delta}{\sqrt{(g\mu_B B - \delta)^2 + \Omega^2}}}. \end{aligned} \tag{A13}$$

The remaining coefficients are vanishing, $B_{1\downarrow} = A_{1\uparrow} = A_{2\downarrow} = B_{2\uparrow} = A_{3\downarrow} = B_{3\uparrow} = B_{4\downarrow} = A_{4\uparrow} = 0$.

b. Zeeman field and SOI axis are parallel ($\theta = 0,\pi$)

In the case of $\theta = 0,\pi$, the SOI is proportional to σ^z. Consequently, we expect the eigenstates of $H_{\mathrm{D}}^{(2)}$ to be mixtures of same spins in different orbitals. For $\theta = 0$, we find that the nonvanishing coefficients are given by

$$B_{1\downarrow} = A_{2\downarrow} = -B_{3\uparrow} = A_{4\uparrow} = \frac{\mathrm{sgn}(\Omega)}{\sqrt{2}}\sqrt{1 - \frac{\delta}{\sqrt{\Omega^2 + \delta^2}}}, \quad A_{1\downarrow} = -B_{2\downarrow} = A_{3\uparrow} = B_{4\uparrow} = \frac{1}{\sqrt{2}}\sqrt{1 + \frac{\delta}{\sqrt{\Omega^2 + \delta^2}}}. \tag{A14}$$

The remaining coefficients are all zero, $B_{1\uparrow} = A_{1\uparrow} = A_{2\uparrow} = B_{2\uparrow} = A_{3\downarrow} = B_{3\downarrow} = B_{4\downarrow} = A_{4\downarrow} = 0$. For $\theta = \pi$, we find find that

$$B_{1\downarrow} = A_{2\downarrow} = -B_{3\uparrow} = A_{4\uparrow} = -\frac{\mathrm{sgn}(\Omega)}{\sqrt{2}}\sqrt{1 - \frac{\delta}{\sqrt{\Omega^2 + \delta^2}}}, \quad A_{1\downarrow} = -B_{2\downarrow} = A_{3\uparrow} = B_{4\uparrow} = \frac{1}{\sqrt{2}}\sqrt{1 + \frac{\delta}{\sqrt{\Omega^2 + \delta^2}}}. \tag{A15}$$

As before, the remaining coefficients vanish, $B_{1\uparrow} = A_{1\uparrow} = A_{2\uparrow} = B_{2\uparrow} = A_{3\downarrow} = B_{3\downarrow} = B_{4\downarrow} = A_{4\downarrow} = 0$.

c. Zeeman field and SOI axis are nonorthogonal and nonparallel ($\theta \neq 0,\pi/2,\pi$)

We assume that $\Omega \neq 0$; for $\Omega = 0$ we note that $H_{\mathrm{D}}^{(1)}$ is already diagonal. When $\theta \neq 0,\pi/2,\pi$, the SOI is proportional to both σ^x and σ^z. This means that the SOI mixes states of all spin species in all orbitals. We find that the components of the respective eigenstates are given by

$$\begin{aligned} B_{1\uparrow} &= \frac{1}{N_1}\frac{g\mu_B B + \sqrt{\delta^2 + (\Omega\,\cos\theta)^2} - \sqrt{(g\mu_B B + \sqrt{\delta^2 + (\Omega\,\cos\theta)^2})^2 + (\Omega\,\sin\theta)^2}}{\Omega\,\sin\theta}, \\ B_{2\uparrow} &= \frac{1}{N_2}\frac{g\mu_B B - \sqrt{\delta^2 - (\Omega\,\cos\theta)^2} - \sqrt{(g\mu_B B - \sqrt{\delta^2 + (\Omega\,\cos\theta)^2})^2 + (\Omega\,\sin\theta)^2}}{\Omega\,\sin\theta}, \\ B_{3\uparrow} &= \frac{1}{N_3}\frac{g\mu_B B - \sqrt{\delta^2 - (\Omega\,\cos\theta)^2} + \sqrt{(g\mu_B B - \sqrt{\delta^2 + (\Omega\,\cos\theta)^2})^2 + (\Omega\,\sin\theta)^2}}{\Omega\,\sin\theta}, \\ B_{4\uparrow} &= \frac{1}{N_4}\frac{g\mu_B B + \sqrt{\delta^2 + (\Omega\,\cos\theta)^2} + \sqrt{(g\mu_B B + \sqrt{\delta^2 + (\Omega\,\cos\theta)^2})^2 + (\Omega\,\sin\theta)^2}}{\Omega\,\sin\theta}, \\ B_{1\downarrow} &= \frac{1}{N_1}\frac{\Omega\,\cos\theta}{\delta + \sqrt{\delta^2 + (\Omega\,\cos\theta)^2}}, \quad B_{4\downarrow} = \frac{1}{N_4}\frac{\Omega\,\cos\theta}{\delta + \sqrt{\delta^2 + (\Omega\,\cos\theta)^2}}, \\ B_{2\downarrow} &= \frac{1}{N_2}\frac{\Omega\,\cos\theta}{\delta - \sqrt{\delta^2 + (\Omega\,\cos\theta)^2}}, \quad B_{3\downarrow} = \frac{1}{N_3}\frac{\Omega\,\cos\theta}{\delta - \sqrt{\delta^2 + (\Omega\,\cos\theta)^2}}, \\ A_{\lambda\uparrow} &= \frac{1}{N_\lambda}B_{\lambda\uparrow}B_{\lambda\downarrow}, \quad A_{\lambda\downarrow} = \frac{1}{N_\lambda}, \end{aligned} \tag{A16}$$

where N_λ is a normalization factor which we choose so that $\sqrt{A_{\lambda\uparrow}^2 + A_{\lambda\downarrow}^2 + B_{\lambda\uparrow}^2 + B_{\lambda\downarrow}^2} = 1$. The normalization also ensures that when $\theta \to 0,\pi/2,\pi$ the expressions above reproduce the the corresponding limiting cases.

APPENDIX B: s-WAVE SUPERCONDUCTOR φ_0 JOSEPHSON JUNCTION

This second section of the appendix gives a more detailed discussion of the SC JJ described by $H_{\rm S}$ in the main text.

1. Effective tunneling Hamiltonian

We begin with a derivation of the effective tunneling Hamiltonian $H_{\rm S,t}^{\rm eff}$. Compared to the main text, we allow for a slightly more general tunneling Hamiltonian with spin-dependent tunneling amplitudes,

$$H_{\rm S,t} = \sum_{\eta\tau}\sum_{\mathbf{k}s} t_{\eta\tau s} e^{i\varphi_\eta/2}\, c^\dagger_{\eta,\mathbf{k}s} d_{\tau s} + \text{H.c.} \tag{B1}$$

Because it is only the relative phase between the two superconductors which is a physical quantity, we assume that $\varphi_2 = 0$ while $\varphi_1 \equiv \varphi$. We now briefly discuss the different tunneling processes which can occur in the system. Therefore, we rewrite $H_{\rm S,t}$ in terms of the quasiparticle operators,

$$\begin{aligned} H_{\rm S,t} = \sum_{\tau}\sum_{\mathbf{k}} & t_{1\tau\uparrow} e^{i\varphi/2} u_{\mathbf{k}} \gamma^\dagger_{1,\mathbf{k}\Uparrow} d_{\tau\uparrow} + t_{1\tau\uparrow} e^{i\varphi/2} v_{\mathbf{k}} \gamma_{1,\mathbf{k}\Downarrow} d_{\tau\uparrow} + t_{2\tau\uparrow} u_{\mathbf{k}} \gamma^\dagger_{2,\mathbf{k}\Uparrow} d_{\tau\uparrow} + t_{2\tau\uparrow} v_{\mathbf{k}} \gamma_{2,\mathbf{k}\Downarrow} d_{\tau\uparrow} \\ & + t_{1\tau\downarrow} e^{i\varphi/2} u_{\mathbf{k}} \gamma^\dagger_{1,\mathbf{k}\Downarrow} d_{\tau\downarrow} - t_{1\tau\downarrow} e^{i\varphi/2} v_{\mathbf{k}} \gamma_{1,\mathbf{k}\Uparrow} d_{\tau\downarrow} + t_{2\tau\downarrow} u_{\mathbf{k}} \gamma^\dagger_{2,\mathbf{k}\Downarrow} d_{\tau\downarrow} - t_{2\tau\downarrow} v_{\mathbf{k}} \gamma_{2,\mathbf{k}\Uparrow} d_{\tau\downarrow} + \text{H.c.}, \end{aligned} \tag{B2}$$

where we have assumed that $\xi_{\mathbf{k}} = \xi_{-\mathbf{k}}$. We see that there are two types of tunneling processes. On the one hand, there are processes in which we destroy an electron on the dot and create a quasiparticle on one of the SC leads (or vice versa). Here, electrons and quasiparticles carry the same type of spin or pseudospin. On the other hand, there are processes in which we use the superconducting condensate to simultaneously create (or destroy) an electron on the dot and a quasiparticle on the SC leads. In this case, electron and quasiparticle always carry the opposite type of spin or pseudospin. Because of our convention for the superconducting phases, whenever we destroy (create) an electron on the dot and destroy or create a quasiparticle on SC $\eta = 1$ we pick up a phase of $e^{i\varphi/2}$ ($e^{-i\varphi/2}$) during the tunneling process.

We now derive the effective tunneling Hamiltonian $H_{\rm S,t}^{\rm eff}$ using the projection method [52]. Up to fourth order in the tunneling amplitudes we find that

$$H_{\rm S,t}^{\rm eff} = P_{\rm S} H_{\rm S,t} (E_-^{(2)} - H_{\rm D} - H_{\rm S,L})^{-1} (1 - P_{\rm S}) H_{\rm S,t}\, P_{\rm S} + P_{\rm S}\, H_{\rm S,t} [(E_-^{(2)} - H_{\rm D} - H_{\rm SC,L})^{-1} (1 - P_{\rm S}) H_{\rm S,t}]^3\, P_{\rm S}, \tag{B3}$$

where $P_{\rm S} = |0_1, E_-^{(2)}, 0_2\rangle\langle 0_1, E_-^{(2)}, 0_2|$ is the projector on the $E_-^{(2)}$ state on the dot and the ground states of the SC leads. It acts within the reduced Hilbert space of the states $E_\pm^{(2)}, E_\lambda^{(1)}$ on the dot and the full Hilbert space of the SC leads. Evaluating Eq. (B3) yields an expression as given by Eq. (6) in the main text with $\nu = \text{S}$ and

$$\begin{aligned} E_{\rm S}^0 &= g_{\rm S} t_{1b\downarrow} t_{2b\downarrow} B^2_{\lambda\uparrow} \big(A^2_{\lambda\uparrow} t_{1b\uparrow} t_{2b\uparrow} + B^2_{\lambda\uparrow} t_{1a\uparrow} t_{2a\uparrow} \big), \\ E_{\rm S}^a &= g_{\rm S} t_{1b\downarrow} t_{2b\downarrow} A_{\lambda\uparrow} B^3_{\lambda\uparrow} \big(t_{1a\uparrow} t_{2b\uparrow} - t_{1b\uparrow} t_{2a\uparrow} \big). \end{aligned} \tag{B4}$$

We point out that, unlike Eq. (8) in the main text, this result holds also for spin-dependent tunneling amplitudes. The coupling constant is given by

$$g_{\rm S} = 2 \sum_{\mathbf{k},\mathbf{q}} \frac{u_{\mathbf{k}} u_{\mathbf{q}} v_{\mathbf{k}} v_{\mathbf{q}}}{\big(E_\lambda^{(1)} + E_{\mathbf{q}} - E_-^{(2)}\big)\big(E_+^{(2)} + E_{\mathbf{k}} + E_{\mathbf{q}} - E_-^{(2)}\big)\big(E_\lambda^{(1)} + E_{\mathbf{k}} - E_-^{(2)}\big)} > 0. \tag{B5}$$

We give a complete table of the tunneling sequences (up to Hermitian conjugation) contributing to the Cooper pair transport in Figs. 3 and 4. Here, we note that the sum of the processes in each row of Fig. 3 and Fig. 4 is $\propto (S_+T_- - S_-T_+)^2$. This factor is unity because the states $E_\pm^{(2)}$ are orthonormal; see Eq. (A8). This explains why the singlet-triplet mixing does not enter the effective tunneling Hamiltonian. We omit the presentation of $\widetilde{E}_{\rm S}$ since it is not relevant to compute the Josephson current. The phase shifts $\varphi_{\rm S}^0(\theta)$ and Josephson currents $I_{\rm S}(\theta)$ at $\varphi_{\rm S} = 0$ are plotted in Fig. 9.

Finally, we highlight that it is sufficient to consider a parabolic normal state dispersion for the topologically trivial superconducting phase, i.e., to neglect the effects of SOI. To see this, recall that in the topologically superconducting phase of the nanowires the chemical potential needs to be carefully tuned inside of the gap opened by the magnetic field, while for typical experiments in the trivial superconducting phase the chemical potential lies well above the gap opened by the magnetic field. In the latter case, the small linear correction of the SOI to the parabolic dispersion of the nanowire becomes practically irrelevant. Hence we do not expect that the SOI axis in the wire has any measurable effect on the anomalous phase offset in the trivial superconducting phase of the wire, i.e., we expect a trivial phase offset in the case when Zeeman field and SOI axis on the dot are orthogonal. This also means that a wire SOI axis that is misaligned with respect to the dot SOI axis will not affect the phase shift of the supercurrent. This argument was also verified by recent experiments, see Ref. [39], which were carried out in the trivial superconducting phase at around 100–200 mT. In these experiments the gates applied to the quantum dot inevitably cause its SOI axis to deviate from the intrinsic wire SOI axis, while at the same time no nontrivial

FIG. 3. Tunneling sequences (up to Hermitian conjugation) of the SC JJ for contributions $\propto \cos\varphi_S$. We use the basis $|n_{1\mathbf{k}\Uparrow}, n_{1\mathbf{k}\Downarrow}, n_{a\uparrow}, n_{a\downarrow}, n_{b\uparrow}, n_{b\downarrow}, n_{2\mathbf{q}\Uparrow}, n_{2\mathbf{q}\Downarrow}\rangle = (\gamma^\dagger_{1\mathbf{k}\Uparrow})^{n_{1\mathbf{k}\Uparrow}} (\gamma^\dagger_{1\mathbf{k}\Downarrow})^{n_{1\mathbf{k}\Downarrow}} (d^\dagger_{a\uparrow})^{n_{a\uparrow}} (d^\dagger_{a\downarrow})^{n_{a\downarrow}} (d^\dagger_{b\uparrow})^{n_{b\uparrow}} (d^\dagger_{b\downarrow})^{n_{b\downarrow}} (\gamma^\dagger_{2\mathbf{q}\Uparrow})^{n_{2\mathbf{q}\Uparrow}} (\gamma^\dagger_{2\mathbf{q}\Downarrow})^{n_{2\mathbf{q}\Downarrow}} |0_1, 0_D, 0_2\rangle$. Filled (empty) dots are used to visually represent a filled (empty) level.

phase offset was measured when Zeeman field and dot SOI axis are orthogonal.

APPENDIX C: TOPOLOGICAL SUPERCONDUCTOR φ_0 JOSEPHSON JUNCTION

1. Effective tunneling Hamiltonian

We devote this third part of the appendix to the derivation and discussion of the effective tunneling Hamiltonian $H^{\text{eff}}_{\text{TS,t}}$ for the TS JJ. Here, the lowest order contribution comes at t^2. This is, roughly, due to the remarkable property of MBSs being their own antiparticle: it takes two steps in a sequence of intermediate states to transfer a nonlocal fermion from the left to the right TS (or vice versa) and to return to the ground state of the quantum dot. This will ensure an enhancement in critical current, for sufficiently small tunneling, and a 4π periodicity of the supercurrent as a function of the phase difference. Also we note that our arguments apply to the effective Hamiltonian containing amplitudes, while a real transport process would be described eventually by probabilities (amplitudes squared).

We now begin with derivation of the effective Hamiltonian for the TS JJ. In general, the tunnel coupling between the SC leads and the QD is described by the tunneling Hamiltonian,

$$H_{\text{t}} = \sum_{\eta} \sum_{s} \int dx\, dx'\, \tilde{t}_{\eta s}(x,x') e^{i\varphi_\eta/2} \Psi^\dagger_{\eta s}(x) d_s(x') + \text{H.c.} \tag{C1}$$

Here, $\Psi^\dagger_{\eta s}(x)$ is the creation operator of an electron with spin s at position x in SC lead η and $d_s(x')$ is the annihilation of an electron with spin s at position x' in the QD. Furthermore, $\tilde{t}_{\eta\tau s}(x,x')$ is the tunneling matrix element. If the leads are topological superconducting leads, we can rewrite the electron operators in the TSs in terms of quasiparticle operators [46],

$$\Psi^\dagger_{\eta s}(x) = \Psi_{\eta s}(x)\Gamma_\eta + \psi'_{\eta s}(x)\Gamma'_\eta + \cdots . \tag{C2}$$

Here, as in the main text, Γ_η is the zero-energy MBS which is localized at the boundary of the TS η that is spatially closest to the QD, while Γ'_η is the zero-energy MBS that is localized at the opposite end. The corresponding MBS wave functions are given by $\psi_\eta(x)$ and $\psi'_\eta(x)$, respectively. Moreover, "$+\cdots$" refers to the contributions of finite-energy quasiparticles, which we neglect as we are interested only in energies much smaller than the energy gap. Similarly, assuming for simplicity that the QD consists of only two orbitals a and b, we can expand the electron operator in the

FIG. 4. Same as Fig. 3 but for contributions $\propto \sin\varphi_S$ to the effective Hamiltonian of the SC JJ.

QD according to

$$d_s(x') = \sum_{\tau=a,b} \xi_{\tau s}(x') d_{\tau s}, \tag{C3}$$

where $d_{\tau s}$ is the annihilation operator of an electron with spin s in orbital τ of the QD and $\xi_{\tau s}(x')$ is the corresponding wave function. Now, we insert the expansions given in Eq. (C2) and Eq. (C3) into Eq. (C1). Assuming that the wave functions of the MBSs Γ'_η have zero overlap with the QD wave functions, this yields the tunneling Hamiltonian given in Eq. (3) of the main text,

$$H_t \to H_{TS,t} = \sum_{\eta\tau} \sum_{s} t_{\eta\tau s} e^{i\varphi_\eta/2}\, \Gamma_\eta d_{\tau s} + \text{H.c.}, \tag{C4}$$

where we have defined new tunneling amplitudes

$$t_{\eta\tau s} = \int dx\, dx'\, \tilde{t}_{\eta s}(x,x') \psi_{\eta s}(x) \xi_{\tau s}(x'). \tag{C5}$$

For simplicity, we will assume that the tunneling amplitudes $t_{\eta\tau s}$ are real. We now derive an effective Hamiltonian considering the tunneling amplitudes as small perturbations. Once more, we emphasize that the lowest order processes which contribute to the Josephson current are of second order in the tunneling amplitudes. In particular these processes do not mix the total fermion parity of the TS leads. Because of that, we focus on the odd parity subspace of the TSs. The results for the even parity subspace of the TSs are identical. The effective tunneling Hamiltonian up to second order in the tunneling amplitudes is given by

$$H^{\text{eff}}_{TS,t} = P_{TS} H_{TS,t} (E^{(2)}_- - H_D - H_{TS,L})^{-1} (1 - P_{TS}) H_{TS,t}\, P_{TS}, \tag{C6}$$

where $P_{TS} = |1_1, E^{(2)}_-, 0_2\rangle\langle 1_1, E^{(2)}_-, 0_2| + |0_1, E^{(2)}_-, 1_2\rangle\langle 0_1, E^{(2)}_-, 1_2|$ is the projector on the $E^{(2)}_-$ state on the dot and the ground states of the TS leads. It acts within the reduced Hilbert space of the states $E^{(2)}_\pm, E^{(1)}_\lambda$ on the dot and the odd parity ground state subspace of the TS leads. In particular, 0_η (1_η) denotes the ground state in which the nonlocal fermionic mode in TS η is unoccupied (occupied). When evaluating Eq. (C6) we find that the result is of the form as given in the main text by

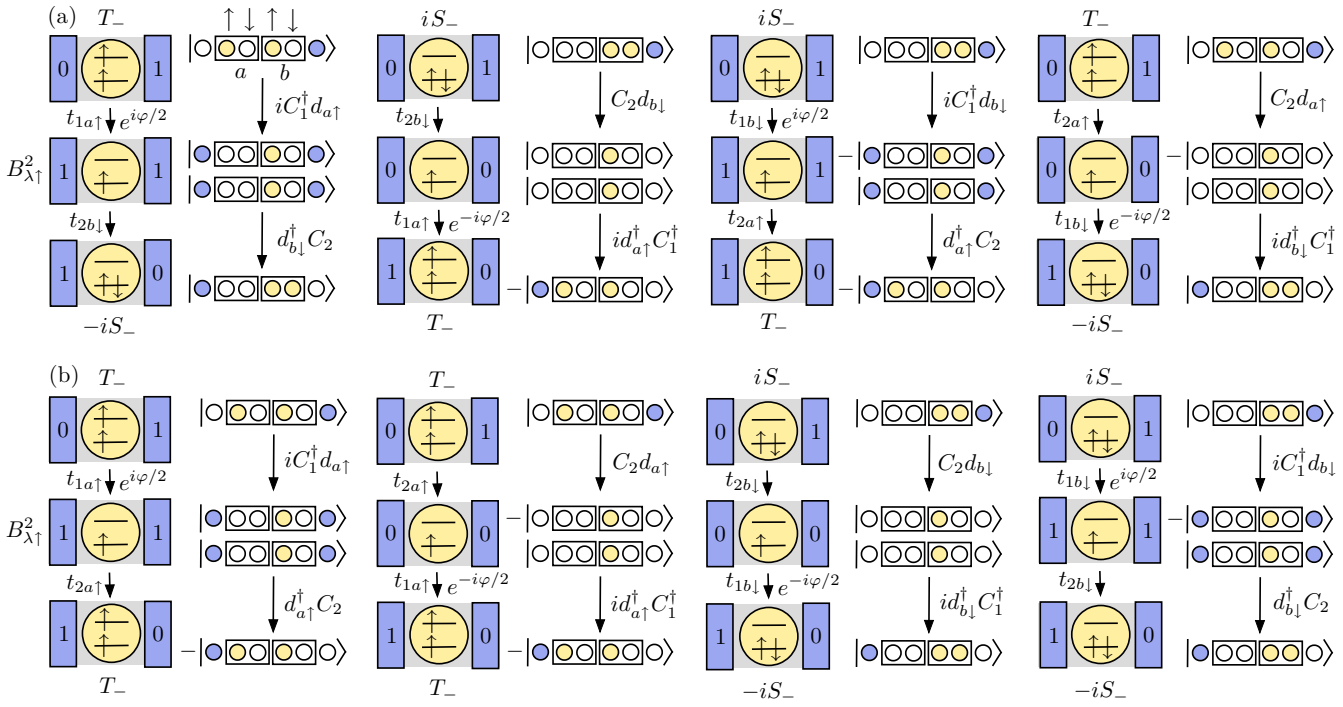

FIG. 5. Tunneling sequences of the TS JJ for $\theta = \pi/2$. We use the basis $|n_1,n_{a\uparrow},n_{a\downarrow},n_{b\uparrow},n_{b\downarrow},n_2\rangle = (C_1^\dagger)^{n_1}(d_{a\uparrow}^\dagger)^{n_{a\uparrow}}(d_{a\downarrow}^\dagger)^{n_{a\downarrow}}(d_{b\uparrow}^\dagger)^{n_{b\uparrow}}(d_{b\downarrow}^\dagger)^{n_{b\downarrow}}(C_2^\dagger)^{n_2}|0_1,0_D,0_2\rangle$. Filled (empty) dots are used to visually represent a filled (an empty) level. (a) Tunneling sequences that give contributions $\propto\cos(\varphi_{TS})$. (b) Tunneling sequences that give contributions $\propto\sin(\varphi_{TS})$.

Eq. (6) with $\nu = \mathrm{TS}$ and

$$\begin{aligned} E^0_{\mathrm{TS}} &= g_{\mathrm{TS}}\big[B_{\lambda\uparrow}T_-(A_{\lambda\uparrow}T_- + B_{\lambda\downarrow}S_-)(t_{1a\uparrow}t_{2b\uparrow} - t_{1b\uparrow}t_{2a\uparrow}) \\ &\quad + B^2_{\lambda\uparrow}S_-T_-(t_{1b\downarrow}t_{2a\uparrow} - t_{1a\uparrow}t_{2b\downarrow})\big], \\ E^a_{\mathrm{TS}} &= -g_{\mathrm{TS}}\big[(A_{\lambda\uparrow}T_- + B_{\lambda\downarrow}S_-)^2 t_{1b\uparrow}t_{2b\uparrow} \\ &\quad + B^2_{\lambda\uparrow}(S^2_-t_{1b\downarrow}t_{2b\downarrow} + T^2_-t_{1a\uparrow}t_{2a\uparrow}) \\ &\quad - B_{\lambda\uparrow}S_-(A_{\lambda\uparrow}T_- + B_{\lambda\downarrow}S_-)(t_{1b\uparrow}t_{2b\downarrow} + t_{1b\downarrow}t_{2b\uparrow})\big], \end{aligned} \tag{C7}$$

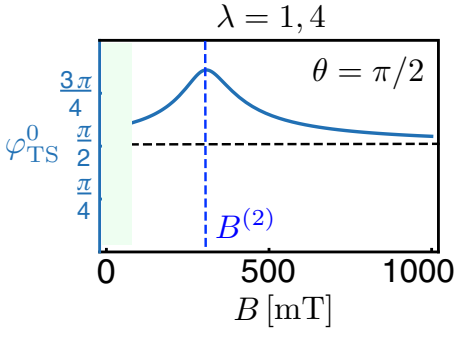

FIG. 6. Phase shift φ^0_{TS} as a function of the magnitude of the external magnetic field B at $\theta = \pi/2$ for $\lambda = 1,4$. For $\lambda = 2,3$ the phase shift is independent of B and given by $\varphi^0_{\mathrm{TS}} = \pi/2$. For the SC JJ we do not observe a phase shift when $\theta = \pi/2$, $\varphi^0_{\mathrm{S}} = 0$. We see that the phase shift is peaked at $B = B^{(2)}$ when the singlet triplet mixing is maximal and it saturates at $\pi/2$ when $B \gg B^{(2)}$. Note however that our perturbative approach is not valid when $B \ll B^{(2)}$, because additional energy levels would have to be taken into account.

where we have introduced the coefficient

$$g_{\mathrm{TS}} = \frac{2}{E^{(1)}_\lambda - E^{(2)}_-} > 0. \tag{C8}$$

There are also processes which do not transport a nonlocal fermion across the JJ and thus lead to a contribution $\widetilde{E}_{\mathrm{TS}}$ which is independent of the superconducting phase difference. In these processes each TS interacts separately with the QD. In particular this means that the action of the effective tunneling Hamiltonian on the two odd parity ground states of the TS is identical. Consequently, this contribution is proportional to the identity operator and is not relevant when computing the zero-temperature Josephson current. For the case when $\theta = \pi/2$ we have listed all the intermediate tunneling sequences

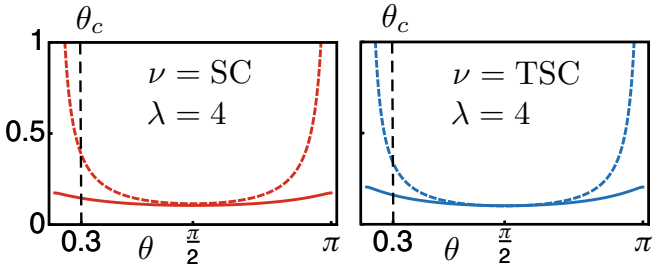

FIG. 7. Estimate of the critical angle θ_c when $\lambda = 4$ by analyzing the conditions for the weak coupling limit as a function of θ. The system parameters are chosen as in the main text and the Appendixes. In the left panel we plot $\pi\nu_F t^2/(\Omega\sin\theta)$ (red dashed) and $\pi\nu_F t^2/|E^{(1)}_4 - E^{(2)}_-|$ (red solid). In the right panel we plot $t/(\Omega\sin\theta)$ (blue dashed) and $t/|E^{(1)}_4 - E^{(2)}_-|$ (blue solid). We find that $\theta_c = 0.3$. This choice of critical angle also works for $\lambda = 1,2,3$.

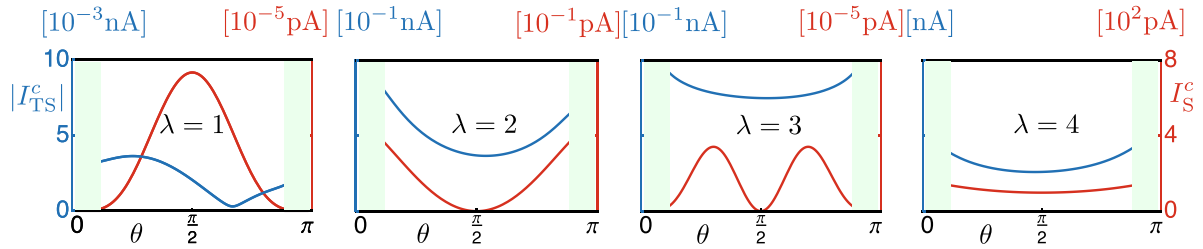

FIG. 8. Magnitude of the critical current $|I_v^c(\theta)|$ for different choices of λ. The system parameters are chosen as in the main text and the Appendixes.

which contribute to the Josephson current in Fig. 5. The phase shift $\varphi_{\rm TS}^0(\theta=\pi/2)$ for $\lambda = 1,4$ is plotted as a function of the external Zeeman field in Fig. 6. The phase shifts $\varphi_{\rm TS}^0(\theta)$ and Josephson currents $I_{\rm TS}(\theta)$ at $\varphi_{\rm TS}=0$ are plotted in Fig. 9.

Lastly, one might think that also finite energy quasiparticles contribute to the effective Hamiltonian. This is indeed true. However, the finite energy quasiparticle sequences of intermediate states which contribute to the Josephson current are of fourth order in the tunneling amplitudes and suppressed by the superconducting gap. Compared to that the Majorana bound state contributions are of second order in tunneling amplitudes. For this reason, we neglect finite energy quasiparticle contributions for the TS-Dot-TS junction when working in the weak tunnel coupling limit.

APPENDIX D: CRITICAL ANGLE

The effective Hamiltonians for the SC JJ and the TS JJ are valid in the weak tunnel coupling limit. For the SC JJ this limit is defined by

$$\pi \nu_F t_{\eta\tau} t_{\eta'\tau'} \ll E_\lambda^{(1)} - E_-^{(2)}, \Omega\,\sin(\theta), \Delta \tag{D1}$$

and for the TS JJ by

$$t_{\eta\tau} \ll E_\lambda^{(1)} - E_-^{(2)}, \Omega\,\sin(\theta). \tag{D2}$$

These conditions fix a critical angle $\theta_c > 0$ so that our perturbative approach is valid when $\theta \in [\theta_c, \pi-\theta_c]$. In this section we want to determine this critical angle for the system parameters which we have chosen in Fig. 3 of the main text. To get a sense of scales, we consider an InAs nanowire QD JJ with SC leads of length $L = 1\ \mu$m. We assume that the effective mass of the electrons in the wire is given by $m = 0.05 m_e$, where m_e is the bare electron mass. Furthermore, we expect that the Fermi energy of the leads is given by $E_F = 0.1$ meV and the induced superconducting gap by $\Delta = 0.1$ meV. The density of states at the Fermi level of the nanowires in the normal metal state is given by $\nu_F = \frac{L}{\pi}\sqrt{\frac{2m}{\hbar^2}}\frac{1}{\sqrt{E_F}}$. For the order of magnitude of the tunnel coupling between dot and leads we assume that $t = 0.01$ meV. Furthermore, we fix V_g so that $E_\lambda^{(1)}(\pi/2) - E_-^{(2)}(\pi/2) \approx 0.1$ meV. This means that depending on the choice of λ we have $(V_g|_{\lambda=1}, V_g|_{\lambda=2}, V_g|_{\lambda=4}, V_g|_{\lambda=4}) = (0.89\text{ meV}, 0.20\text{ meV}, -0.12\text{ meV}, -0.80\text{ meV})$. We can now graphically find an estimate for θ_c; see Fig. 7. A choice of critical angle that works for all λ is given by $\theta_c = 0.3$.

APPENDIX E: CRITICAL CURRENTS

1. Critical current of the SC JJ

In this section of the appendix we compute the critical current $I_{S,c}$. First, we need to find an approximate value for the coefficient g_S. To this end, we notice that it can be rewritten as

$$g_S = \frac{\Delta^2}{2}\int_{-\hbar\omega_c}^{\hbar\omega_c}\nu(E_1)dE_1\int_{-\hbar\omega_c}^{\hbar\omega_c}\nu(E_2)dE_2\frac{1}{\sqrt{E_1^2+\Delta^2}\sqrt{E_2^2+\Delta^2}} \times \frac{1}{\left[\left(E_{\lambda_0}^{(1)}-E_-^{(2)}\right)+\sqrt{E_1^2+\Delta^2}\right]\left[\left(E_{\lambda_0}^{(1)}-E_-^{(2)}\right)+\sqrt{E_2^2+\Delta^2}\right]\left[\left(E_+^{(2)}-E_-^{(2)}\right)+\sqrt{E_1^2+\Delta^2}+\sqrt{E_2^2+\Delta^2}\right]}, \tag{E1}$$

where $\nu(E) = \sum_{\mathbf{k}}\delta(E-E_{\mathbf{k}})$ is the density of state of the leads in the normal state at energy E and ω_c is a cutoff frequency which is typically of the order of the Debye frequency of the crystal. For simplicity, we now assume that $\nu(E) \approx \nu_F$ for $|E| \geqslant \Delta$ and $\nu(E) = 0$ for $|E| < \Delta$. This yields

$$g_S \approx \frac{(\Delta\nu_F)^2}{2}\left(\int_{-\hbar\omega_c}^{-\Delta}dE_1+\int_{\Delta}^{\hbar\omega_c}dE_1\right)\left(\int_{-\hbar\omega_c}^{-\Delta}dE_2+\int_{\Delta}^{\hbar\omega_c}dE_2\right)\frac{1}{\sqrt{E_1^2+\Delta^2}\sqrt{E_2^2+\Delta^2}} \times \frac{1}{\left[\left(E_{\lambda_0}^{(1)}-E_-^{(2)}\right)+\sqrt{E_1^2+\Delta^2}\right]\left[\left(E_{\lambda_0}^{(1)}-E_-^{(2)}\right)+\sqrt{E_2^2+\Delta^2}\right]\left[\left(E_+^{(2)}-E_-^{(2)}\right)+\sqrt{E_1^2+\Delta^2}+\sqrt{E_2^2+\Delta^2}\right]}. \tag{E2}$$

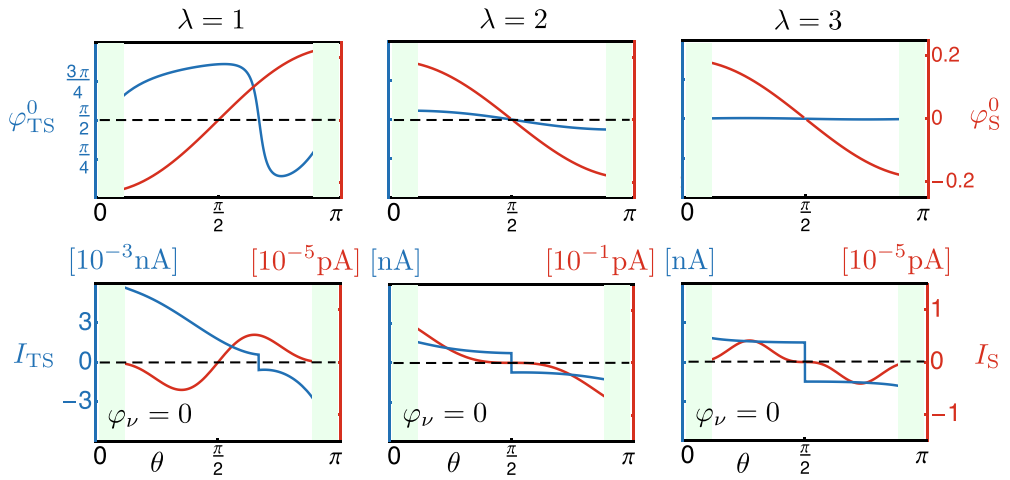

FIG. 9. Phase shift $\varphi^0_\nu(\theta)$ (top row) and Josephson current $I_\nu(\theta)$ at $\varphi_{\rm S} = 0$ (bottom row) for $\lambda = 1,2,3$. The system parameters are chosen as in the main text. The jumps in the Josephson current $I_{\rm TS}(\theta)$ correspond to a change of the ground state of the junction.

Defining $\xi_\pm = (E^{(1)}_\lambda - E^{(2)}_\pm)/\Delta$ allows us to rewrite this expression as

$$g_{\rm S} \approx \frac{4\alpha}{\pi^2}\frac{mL^2}{\hbar^2\Delta E_F}, \tag{E3}$$

where we have introduced the dimensionless factor

$$\alpha = \int_1^\infty dx \int_1^\infty dy \, \frac{1}{\sqrt{1+x^2}\sqrt{1+y^2}(\sqrt{1+x^2}+\sqrt{1+y^2}+\xi_- - \xi_+)(\sqrt{1+x^2}+\xi_-)(\sqrt{1+y^2}+\xi_-)} \tag{E4}$$

and we have assumed that $\hbar\omega_c \gg \Delta$ which ensures that the Cooper potential of the BCS theory is a good approximation to the actual electron pairing potential. We note that α is a function of the relative orientation of SOI axis and Zeeman field, $\alpha = \alpha(\theta)$. For the system parameters chosen in the main text we find that $\alpha \approx 10^{-1}$. In total the critical current is then given by

$$I^c_{\rm S} \approx \frac{8\alpha}{\pi^2}\frac{meL^2}{\hbar^3\Delta E_F}\sqrt{\left(E^0_{\rm S}\right)^2 + \left(E^a_{\rm S}\right)^2}\,\mathrm{sgn}\left(E^0_{\rm S}\right). \tag{E5}$$

We have plotted $I^c_{\rm S}(\theta)$ in Fig. 8. For the case when $\theta = \pi/2$ and $\lambda = 2,3$ we have $I^c_{\rm S} = 0$ because $B_{2(3)\uparrow} = 0$. Moreover, there exists a significant difference in magnitude of the critical currents for the cases when $\lambda = 1,4$ which are most relevant for our experimental proposal in the main text. We can understand this because $I_{{\rm S},c}|_{\lambda=1}/I_{{\rm S},c}|_{\lambda=4} \propto (B_{1\uparrow}/B_{4\uparrow})^4 \approx 10^{-6}$: the virtual state $E^{(1)}_1$ only contains a small amount of $B_{1\uparrow}$ due to the SOI, while $E^{(1)}_4$ consists mostly of $B_{4\uparrow}$; hence $B_{4\uparrow} \gg B_{1\uparrow}$. The conclusion is that the absence or presence of a phase shift can most easily be measured when virtual tunneling occurs via the $E^{(1)}_4$ state. (See Fig. 9 and Fig. 2(a) in the main text.)

2. Critical current of the TS JJ

For the TS JJ we find that the critical current is given by

$$I^c_{\rm TS} = \frac{4\kappa_{\rm TS}e}{\hbar\left(E^{(1)}_{\lambda_0} - E^{(2)}_-\right)}\sqrt{\left(E^0_{\rm TS}\right)^2 + \left(E^a_{\rm TS}\right)^2}\,\mathrm{sgn}\left(E^0_{\rm TS}\right). \tag{E6}$$

We plot $I^c_{\rm TS}(\theta)$ in Fig. 8. Again we see a significant difference in magnitude when comparing the most relevant cases of $\lambda = 1$ and $\lambda = 4$. This can be explained in the same way as for the SC JJ. However, this time we have for example at $\theta = \pi/2$, $I_{{\rm TS},c}|_{\lambda=1}/I_{{\rm TS},c}|_{\lambda=4} \propto (B_{1\uparrow}/B_{4\uparrow})^2 \approx 10^{-3}$.

[1] C. Nayak, S. H. Simon, A. Stern, M. Freedman, and S. Das Sarma, Rev. Mod. Phys. **80**, 1083 (2008).
[2] J. Alicea, Rep. Prog. Phys. **75**, 076501 (2012).
[3] R. M. Lutchyn, J. D. Sau, and S. Das Sarma, Phys. Rev. Lett. **105**, 077001 (2010).
[4] Y. Oreg, G. Refael, and F. von Oppen, Phys. Rev. Lett. **105**, 177002 (2010).
[5] J. Klinovaja and D. Loss, Phys. Rev. B **86**, 085408 (2012).
[6] V. Mourik, K. Zuo, S. M. Frolov, S. R. Plissard, E. P. A. M. Bakkers, and L. P. Kouwenhoven, Science **336**, 1003 (2012).

[7] S. Nadj-Perge, I. K. Drozdov, B. A. Bernevig, and A. Yazdani, Phys. Rev. B **88**, 020407 (2013).

[8] F. Pientka, L. I. Glazman, and F. von Oppen, Phys. Rev. B **88**, 155420 (2013).

[9] S. Nadj-Perge, I. K. Drozdov, J. Li, H. Chen, S. Jeon, Ju. Seo, A. H. MacDonald, B. A. Bernevig, and A. Yazdani, Science **346**, 602 (2014).

[10] R. Pawlak, M. Kisiel, J. Klinovaja, T. Meier, S. Kawai, T. Glatzel, D. Loss, and E. Meyer, npj Quant. Inf. **2**, 16035 (2016).

[11] L. Fu and C. L. Kane, Phys. Rev. Lett. **100**, 096407 (2008).

[12] S. Hart, H. Ren, T. Wagner, P. Leubner, M. Muhlbauer, C. Brune, H. Buhmann, L. W. Molenkamp, and A. Yacoby, Nat. Phys. **10**, 638 (2014).

[13] V. S. Pribiag, A. J. A. Beukman, F. Qu, M. C. Cassidy, C. Charpentier, W. Wegscheider, and L. P. Kouwenhoven, Nat. Nanotechnol. **10**, 593 (2015).

[14] J. Wiedenmann, E. Bocquillon, R. S. Deacon, S. Hartinger, O. Herrmann, T. M. Klapwijk, L. Maier, C. Ames, C. Brune, C. Gould, A. Oiwa, K. Ishibashi, S. Tarucha, H. Buhmann, and L. W. Molenkamp, Nat. Commun. **7**, 10303 (2016).

[15] E. Bocquillon, R. S. Deacon, J. Wiedenmann, P. Leubner, T. M. Klapwijk, C. Brüne, K. Ishibashi, H. Buhmann, and L. W. Molenkamp, Nat. Nanotechnol. **12**, 137 (2017).

[16] R. S. Deacon, J. Wiedenmann, E. Bocquillon, T. M. Klapwijk, P. Leubner, C. Brne, S. Tarucha, K. Ishibashi, H. Buhmann, and L. W. Molenkamp, Phys. Rev. X **7**, 021011 (2017).

[17] V. B. Geshkenbein and A. I. Larkin, Pis'ma Zh. Eksp. Teor. Fiz. **43**, 306 (1986) [JETP Lett. **43**, 395 (1986)].

[18] S. Yip, Phys. Rev. B **52**, 3087 (1995).

[19] M. Sigrist, Prog. Theor. Phys. **99**, 899 (1998).

[20] S. Kashiwaya and Y. Tanaka, Rep. Prog. Phys. **63**, 1641 (2000).

[21] Y. Asano, Y. Tanaka, M. Sigrist, and S. Kashiwaya, Phys. Rev. B **71**, 214501 (2005).

[22] Y. Avishai and T. K. Ng, Phys. Rev. B **81**, 104501 (2010).

[23] A. Buzdin, Phys. Rev. Lett. **101**, 107005 (2008).

[24] J.-F. Liu and K. S. Chan, Phys. Rev. B **82**, 184533 (2010).

[25] E. Goldobin, D. Koelle, R. Kleiner, and R. G. Mints, Phys. Rev. Lett. **107**, 227001 (2011).

[26] H. Sickinger, A. Lipman, M. Weides, R. G. Mints, H. Kohlstedt, D. Koelle, R. Kleiner, and E. Goldobin, Phys. Rev. Lett. **109**, 107002 (2012).

[27] A. A. Reynoso, G. Usaj, C. A. Balseiro, D. Feinberg, and M. Avignon, Phys. Rev. Lett. **101**, 107001 (2008).

[28] F. Dolcini, M. Houzet, and J. S. Meyer, Phys. Rev. B **92**, 035428 (2015).

[29] T. Yokoyama, M. Eto, and Y. V. Nazarov, Phys. Rev. B **89**, 195407 (2014).

[30] G. Campagnano, P. Lucignano, D. Giuliano, and A. Tagliacozzo, J. Phys.: Condens. Matter **27**, 205301 (2015).

[31] J. Klinovaja and D. Loss, Eur. Phys. J. B **88**, 62 (2015).

[32] M. Alidoust and J. Linder, Phys. Rev. B **87**, 060503 (2013).

[33] F. S. Bergeret and I. V. Tokatly, Europhys. Lett. **110**, 57005 (2015).

[34] R. G. Mints, Phys. Rev. B **57**, R3221(R) (1998).

[35] K. N. Nesterov, M. Houzet, and J. S. Meyer, Phys. Rev. B **93**, 174502 (2016).

[36] L. Dell'Anna, A. Zazunov, R. Egger, and T. Martin, Phys. Rev. B **75**, 085305 (2007).

[37] A. Zazunov, R. Egger, T. Jonckheere, and T. Martin, Phys. Rev. Lett. **103**, 147004 (2009).

[38] A. Brunetti, A. Zazunov, A. Kundu, and R. Egger, Phys. Rev. B **88**, 144515 (2013).

[39] D. B. Szombati, S. Nadj-Perge, D. Car, S. R. Plissard, E. P. A. M. Bakkers, and L. P. Kouwenhoven, Nat. Phys. **12**, 568 (2016).

[40] A. Rasmussen, J. Danon, H. Suominen, F. Nichele, M. Kjaergaard, and K. Flensberg, Phys. Rev. B **93**, 155406 (2016).

[41] J. A. van Dam, Y. V. Nazarov, E. P. A. M. Bakkers, S. De Franceschi, and L. P. Kouwenhoven, Nature (London) **442**, 667 (2006).

[42] B. I. Spivak and S. A. Kivelson, Phys. Rev. B **43**, 3740 (1991).

[43] C. Schrade, A. A. Zyuzin, J. Klinovaja, and D. Loss, Phys. Rev. Lett. **115**, 237001 (2015).

[44] S. Hoffman, C. Schrade, J. Klinovaja, and D. Loss, Phys. Rev. B **94**, 045316 (2016).

[45] M.-S. Choi, C. Bruder, and D. Loss, Phys. Rev. B **62**, 13569 (2000).

[46] M. Lee, J. S. Lim, and R. Lopez, Phys. Rev. B **87**, 241402(R) (2013).

[47] B. Béri, Phys. Rev. Lett. **110**, 216803 (2013).

[48] L. A. Landau, S. Plugge, E. Sela, A. Altland, S. M. Albrecht, and R. Egger, Phys. Rev. Lett. **116**, 050501 (2016).

[49] C. Fasth, A. Fuhrer, L. Samuelson, V. N. Golovach, and D. Loss, Phys. Rev. Lett. **98**, 266801 (2007).

[50] D. J. van Woerkom, A. Geresdi, and L. P. Kouwenhoven, Nat. Phys. **11**, 547 (2015).

[51] Ö. Gül, H. Zhang, F. K. de Vries, J. van Veen, K. Zuo, V. Mourik, S. Conesa-Boj, M. P. Nowak, D. J. van Woerkom, M. Quintero-Pérez, M. C. Cassidy, A. Geresdi, S. Kölling, D. Car, Sé R. Plissard, E. P. A. M. Bakkers, and L. P. Kouwenhoven, Nano Lett. **17**, 2690 (2017).

[52] A. Auerbach, *Interacting Electrons and Quantum Magnetism* (Springer-Verlag, Berlin, 1994).